Available online at www.sciencedirect.com
SCIENCE DIRECT®
Journal of Sound and Vibration 288 (2005) 57–79
JOURNAL OF SOUND AND VIBRATION
www.elsevier.com/locate/jsvi

Transfer function methods to measure dynamic mechanical properties of complex structures

Junhong Park*

School of Mechanical Engineering, Hanyang University, 17 Haengdang-dong, Seongdong-gu, Seoul, 133-791, South Korea

Received 30 January 2004; received in revised form 12 November 2004; accepted 17 December 2004
Available online 11 March 2005

Abstract

Experimental methods to measure frequency-dependent dynamic properties of complex structures are proposed. Flexural wave propagations are analyzed using the Timoshenko beam, the classical beam, and the shear beam theories. Wave speeds, bending and shear stiffnesses of the structures are measured through the transfer function method requiring small number of vibration measurements. Sensitivity analysis to investigate the effects of experimental variables on the measured properties and to study optimal sensor locations of the vibration measurements is performed. Using the developed methods, the complex bending and shear stiffnesses of sandwich beams of different core materials and a polymer beam are measured. Continuous variations of the measured bending and shear stiffnesses and their loss factors with frequency were obtained. To further illustrate the measurements of frequency-dependent variation of dynamic properties of complex structures, the damping of structural vibration using porous and granular materials is investigated. A proper equation of motion for the structural vibration should be used to obtain reliable data. For example, the method of the Timoshenko beam is required when the bending and shear modes of vibration occur simultaneously as in the sandwich beam. With advantages from the flexibility in choosing the vibration measurement locations, the developed methods can be applied to measure dynamic properties of various complex structures and viscoelastic materials.

*Tel.: +82 2 2290 0424.
E-mail address: parkj@hanyang.ac.kr.

0022-460X/$ - see front matter © 2005 Elsevier Ltd. All rights reserved.
doi:10.1016/j.jsv.2004.12.019

Nomenclature

$\hat{A}_1, \hat{A}_2, \hat{A}_3, \hat{A}_4$ complex amplitudes (m)
$\hat{b} = b_r - \mathrm{i}b_i$ frequency parameter
$\hat{c} = c(1 + \mathrm{i}\eta_c), c_b, c_s$ flexural, bending and shear wave speeds (m/s)
$\hat{D} = D(1 + \mathrm{i}\eta_D)$ bending stiffness per unit length (N m^2)
$\hat{E} = E(1 + \mathrm{i}\eta_E)$ complex moduli (Pa)
f frequency (Hz)
$\hat{k}_b = k_{br} - \mathrm{i}k_{bi}$ wavenumber (rad/m)
L length of beam (m)
M_b, I_b mass and rotary inertia per unit length (kg/m, kg m)
$\hat{S} = S(1 + \mathrm{i}\eta_S)$ shear stiffness per unit length (N)
w beam displacements (m)
x_1, x_2 coordinates of vibration measurements (m)
$\hat{\alpha}, \hat{\beta}, \hat{k}_1, \hat{k}_2, r, \hat{s} = s_r + \mathrm{i}s_i$ parameters in Timoshenko beam functions
$\eta_E, \eta_c, \eta_D, \eta_S$ loss factors
A_1, A_2, ϕ_1, ϕ_2 magnitudes and phases of measured transfer functions
ω circular frequency (rad/s)
ψ_x angular rotation

Subscript

j integer

1. Introduction

To investigate structural response excited by non-constant, time-varying external loads, it is required to measure dynamic mechanical properties. The measurement results are useful in design stages, to estimate structural response, sound transmission characteristics, and fatigue life. Recently, the use of the composite honeycomb panels has expanded especially in aerospace applications [1]. The composite honeycomb panel consisting of thin, stiff face materials and a lightweight honeycomb core yields a flexural rigidity that is much larger than the homogeneous plate of equal mass. Due to this increased stiffness with lighter weight, it is beginning to be used as a material in aircraft fuselages. Since large variation of the face and core materials is possible, a simple but reliable test method to measure and compare dynamic mechanical properties is necessary especially when the frequency-dependent variation of the properties are expected.

Widely used methods to measure the dynamic mechanical properties are the resonance tests [2] as adopted for several commercially available dynamic material test systems. In the resonance tests, one method of estimating the damping in the system is using the quality factor [3] to minimize effects from experimental uncertainties. Nevertheless, the frequency range of these devices is commonly limited to frequencies less than 200 Hz. Then, material properties at higher frequencies are obtained by measurements over a range of temperature, and subsequent extrapolation of measured low-frequency data to high frequencies using the WLF (Williams, Landel, and Ferry) equation [4]. Alternatively, several laboratory methods have been proposed to directly measure the dynamic mechanical properties of materials at high frequencies without extrapolation. Madigosky and Lee [5] used a wave propagation approach to measure Young's modulus and the loss factor for frequencies upto 10 kHz. In this method the length of the specimens is required to be large in order to prevent resonance as it is assumed that there are no reflections from the end of the sample. This requirement limits the applicability of the method to materials in which the damping is large and rather long specimens can be obtained.

A measurement method based on standing longitudinal waves was proposed to measure dynamic properties of polymers [6–12]. A rod-like specimen was excited longitudinally, and the elastic modulus and the loss factor were calculated from the transfer function measured between the two accelerometers located at both ends of the specimen. This measurement method was eventually adopted as an ANSI standard [13]. However, these methods are applicable to homogeneous specimens only in the direction of the longitudinal vibration, and are not suitable for measuring the dynamic properties of complex structures under different modes of vibration such as simultaneous bending and shear deformations of the honeycomb panel; Fig. 1.

1D beam theory has been used to determine dynamic mechanical properties of complex structures. The complex moduli of viscoelastic materials were estimated by measuring the resonance frequencies of beams [2], when the viscoelastic materials were used as damping treatments. The measured values were extrapolated to high frequencies using the WLF equation. Again, these techniques may apply only to polymers with distinct temperature and frequency dependences of the dynamic properties. Bland and Lee [14] used a classical beam theory and the transfer function method to calculate the complex stiffness of structures. The beam with clamped–free or clamped–loaded boundary conditions was analyzed. Approximate solutions were proposed to solve the equation formed by the predicted and the measured transfer functions of the beam vibrations.

Several approaches have been proposed to measure the complex wavenumber of beam structures. Rizzi and Doyle [15] measured the wave propagation characteristics of composite beams. Assuming the classical lamination theory, the dynamic bending stiffness and Poisson's ratio were obtained. Measurement techniques using moving averages were used to minimize effects from reflection of propagating waves. Data-processing techniques using the Prony method have been used to measure complex wavenumber, for example the work by Grosh and Williams [16]. This technique requires evenly spaced and relatively large number of data measurements. For smaller number of measurements, an inverse process [17] and nonlinear optimization techniques of minimizing the normalized mean square error between measurements and predictions [18,19] have been proposed to estimate the complex wavenumber. When the shear deformation is not small, for example the sandwich beams, the Timoshenko beam or higher-order beam theories are required to analyze the wave propagations. For the Timoshenko beam, the dynamic mechanical

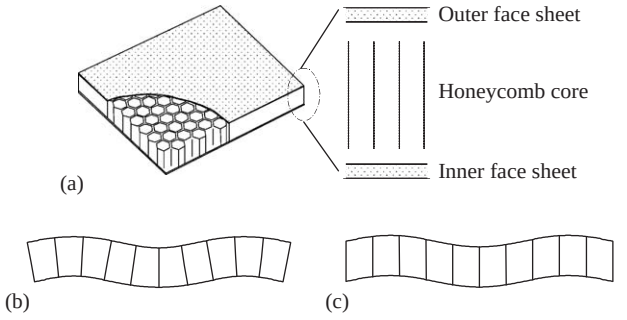

Fig. 1. (a) Schematics of sandwich honeycomb panel and its two different vibrational modes of (b) bending and (c) shear deformations.

properties have been estimated from the modal response by minimizing the error between the measured and predicted resonant frequencies [20–22].

Until now, the transfer function methods have been applied to longitudinal vibration of viscoelastic materials. For the bending vibrations of the classical beam, only an approximate solution has been proposed [14]. When the bending and shear modes of vibration (Fig. 1) occurs simultaneously as in the Timoshenko beam, the estimation of the dynamic properties from the measured transfer function has been done through numerical methods such as the least-squares methods [20–22]. In this study, the transfer function methods are proposed to measure dynamic mechanical properties of complex structures by analyzing the wave propagations using the Timoshenko beam, the classical beam, and the shear beam theories. The results of each approach are compared to each other. Several different boundary conditions, mostly geometric boundary conditions, are considered in deriving and measuring the transfer functions. The wave speed, shear and bending stiffnesses, and their loss factors are measured. The sensitivity of the proposed methods is calculated to study the dependence of the results on vibration characteristics, locations of the vibration measurements, and other experimental variables. The proposed transfer function methods are applied to measure dynamic properties of the three sandwich beams constructed using different core materials and one polymer beam. The slip table tests and the impact hammer tests are performed. From the measured properties and their frequency dependences, the vibrational modes of the structures are estimated. The developed method is applied to investigate the damping of the structural vibration through porous and granular materials—the dynamic bending stiffness of hollow cylindrical beams containing different damping materials is measured. Since the developed transfer function methods are based on the exact solutions, it requires small number of measurements but reliable test results are obtained.

2. Transfer function methods

2.1. Complex bending and shear stiffnesses

To model the dissipation of vibration energy within a structure, complex elastic moduli is used to describe the dynamic mechanical properties. For uniaxial vibrations, the complex modulus is defined as [23]

$$\hat{E}(\omega) = \hat{\sigma}_z(\omega)/\hat{\varepsilon}_z(\omega) = E(\omega)[1 + \mathrm{i}\eta_E(\omega)], \tag{1}$$

where E is the dynamic moduli, η_E is the loss factor, and $\mathrm{i} = \sqrt{-1}$. The Fourier transforms of the stress and the strain are defined as $\hat{\sigma}_z(\omega) = \int_{-\infty}^{\infty} \sigma_z(t)\mathrm{e}^{-\mathrm{i}\omega t}\,\mathrm{d}t$ and $\hat{\varepsilon}_z(\omega) = \int_{-\infty}^{\infty} \varepsilon_z(t)\mathrm{e}^{-\mathrm{i}\omega t}\,\mathrm{d}t$. This definition of the complex modulus applies also to the bending and shear stiffnesses as

$$\hat{D}(\omega) = D(\omega)[1 + \mathrm{i}\eta_D(\omega)], \quad \hat{S}(\omega) = S(\omega)[1 + \mathrm{i}\eta_S(\omega)]. \tag{2}$$

The transfer function method has been applied to longitudinal vibration of rods [6–12]. In this case the direction of the wave propagation and the vibration are identical as shown in Fig. 2(a), and the size of the vibration measurement sensor has no impact on the results if the mass of the sensor is taken into consideration. For flexural vibration, the wave propagation direction is perpendicular to the direction of the vibration as shown in Figs. 2(b) and (c) which show vibrating

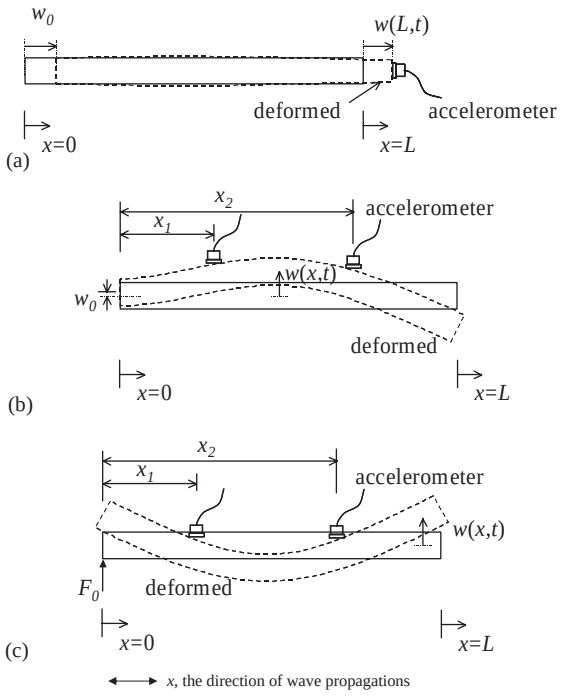

Fig. 2. Measurements of vibration using accelerometers for (a) longitudinal vibrations, and flexural vibrations of (b) clamped–free beam and (c) free–free beam.

beams under two different boundary conditions. The flexural waves generated from external excitations propagate in the x-direction and are reflected and propagate back from boundaries. In this case, the size of the sensor should be as small as possible to avoid problems related to spatially averaged measurements of the wave motion. As vibration measurement sensors with small mass and size, such as miniature piezoelectric accelerometers, MEMS accelerometers, or laser vibrometers, become available, spatial averaging effects and mass loading on the structure are minimized. In this study, miniature piezoelectric accelerometers were used. The mass of the sensor is neglected, and the size is assumed to be negligibly small in deriving the predictions of the transfer functions between the beam displacement.

2.2. The Timoshenko beam

Fig. 2(b) shows the transverse vibration of the beam under fixed–free boundary conditions. The displacement boundary condition is imposed at the clamped edge of the beam. The equation of motion for the Timoshenko beam is

$$D\,\frac{\partial^2\psi_x}{\partial x^2}+S\left(\frac{\partial w}{\partial x}-\psi_x\right)-I_b\,\frac{\partial^2\psi_x}{\partial t^2}=0,\quad M_b\,\frac{\partial^2 w}{\partial t^2}-S\left(\frac{\partial^2 w}{\partial x^2}-\frac{\partial\psi_x}{\partial x}\right)=0, \tag{3a,b}$$

where ψ_x is the angular rotation, M_b and I_b are the mass and rotary inertia per unit length, respectively. The general solution for the Timoshenko beam is well known [24]. In this study, the

satisfying Timoshenko beam functions are given as

$$\hat{w}(x) = \hat{A}_1 \sin \hat{b}\hat{\beta}x + \hat{A}_2 \cos \hat{b}\hat{\beta}x + \hat{A}_3 e^{\hat{b}\hat{\alpha}(x-L)} + \hat{A}_4 e^{-\hat{b}\hat{\alpha}x}, \tag{4a}$$

$$\hat{\psi}_x(x) = \hat{A}_1\hat{k}_1 \cos \hat{b}\hat{\beta}x - \hat{A}_2\hat{k}_1 \sin \hat{b}\hat{\beta}x + \hat{A}_3\hat{k}_2 e^{\hat{b}\hat{\alpha}(x-L)} - \hat{A}_4\hat{k}_2 e^{-\hat{b}\hat{\alpha}x}, \tag{4b}$$

where

$$\begin{pmatrix} \hat{\alpha} \\ \hat{\beta} \end{pmatrix} = \frac{1}{\sqrt{2}} \left\{ \mp[r^2 + \hat{s}^2] + \left[(r^2 - \hat{s}^2)^2 + \frac{4}{\hat{b}^2} \right]^{1/2} \right\}^{1/2},$$

$$r^2 = I_b/M_b, \quad \hat{s}^2 = \hat{D}/\hat{S}, \quad \hat{k}_1 = \hat{b}(\hat{\beta}_2 - \hat{s}^2)/\hat{\beta}, \quad \hat{k}_2 = \hat{b}(\hat{\alpha}^2 + \hat{s}^2)/\hat{\alpha}.$$

The usual complex notation is used, $w(x,t) = \mathrm{Re}\{\hat{w}(x)e^{i\omega t}\}$. Notations of the symbols follow closely those in Ref. [24]. The frequency parameter, $\hat{b}$, is related to the circular frequency through $\hat{b}^2 = \omega^2 M_b/\hat{D}$. Four boundary conditions of the beam in Fig. 2(b) are applied as

$$\hat{w}(0) = w_0, \quad \hat{\psi}_x(0) = 0, \quad \frac{\partial \hat{w}(L)}{\partial x} - \hat{\psi}_x(L) = 0, \quad \frac{\partial \hat{\psi}_x(L)}{\partial x} = 0. \tag{5a–d}$$

Consequently, the following matrix system of equations is obtained as

$$\begin{bmatrix} 0 & 1 & e^{-\hat{b}\hat{\alpha}L} & 1 \\ \hat{k}_1 & 0 & \hat{k}_2 e^{-\hat{b}\hat{\alpha}L} & -\hat{k}_2 \\ \hat{b}\hat{\beta}\cos \hat{b}\hat{\beta}L - \hat{k}_1 \cos \hat{b}\hat{\beta}L & -\hat{b}\hat{\beta}\sin \hat{b}\hat{\beta}L + \hat{k}_1 \sin \hat{b}\hat{\beta}L & +\hat{b}\hat{\alpha} - \hat{k}_2 & -\hat{b}\hat{\alpha}e^{-\hat{b}\hat{\alpha}L} + \hat{k}_2 e^{-\hat{b}\hat{\alpha}L} \\ -\hat{k}_1\hat{b}\hat{\beta}\sin \hat{b}\hat{\beta}L & -\hat{k}_1\hat{b}\hat{\beta}\cos \hat{b}\hat{\beta}L & +\hat{k}_2\hat{b}\hat{\alpha} & +\hat{k}_2\hat{b}\hat{\alpha}e^{-\hat{b}\hat{\alpha}L} \end{bmatrix} \begin{bmatrix} \hat{A}_1 \\ \hat{A}_2 \\ \hat{A}_3 \\ \hat{A}_4 \end{bmatrix}$$

$$= \begin{bmatrix} w_0 \\ 0 \\ 0 \\ 0 \end{bmatrix}. \tag{6}$$

The above matrix system of equations is solved using symbolic calculations to determine the transfer functions of the transverse vibrations. Note that the transfer function of the displacement is same to that of the acceleration. For the transfer function method, the complex wavenumber of the frequency parameter is calculated from the measured transfer functions to obtain the dynamic mechanical properties. For the vibrating Timoshenko beam, the unknown frequency parameters, $\hat{b}$ and $\hat{s}$, are calculated to determine the bending and shear stiffness such that:

$$\hat{D} = \omega^2 M_b/\hat{b}^2, \quad \hat{S} = \omega^2 M_b/\hat{b}^2\hat{s}^2. \tag{7a,b}$$

The calculation requires two different sets of transfer function measurements. The transfer functions between the transverse displacements and the angular rotations, i.e., $\hat{w}(x_1)/\hat{w}(0)$ and $\hat{\psi}_x(x_1)/\hat{w}(0)$, where x_1 is the location of the vibration measurements maybe used. However the angular rotations are more difficult to measure compared to the transverse displacements. In this

study, two different transfer functions of the displacements are used instead as

$$\Lambda_1 e^{i\phi_1} = (\hat{A}_1 \sin \hat{b}\hat{\beta}x_1 + \hat{A}_2 \cos \hat{b}\hat{\beta}x_1 + \hat{A}_3 e^{\hat{b}\hat{\alpha}(x_1-L)} + \hat{A}_4 e^{-\hat{b}\hat{\alpha}x_1})/w_0, \tag{8a}$$

$$\Lambda_2 e^{i\phi_2} = (\hat{A}_1 \sin \hat{b}\hat{\beta}x_2 + \hat{A}_2 \cos \hat{b}\hat{\beta}x_2 + \hat{A}_3 e^{\hat{b}\hat{\alpha}(x_2-L)} + \hat{A}_4 e^{-\hat{b}\hat{\alpha}x_2})/w_0, \tag{8b}$$

where Λ_1 and Λ_2 are the amplitudes and ϕ_1 and ϕ_2 are the phases of the measured transfer functions between the displacement at $x = x_0$ (w_0) and those at $x = x_1$ and x_2 respectively. Eq. (8) is solved numerically using the Newton–Rapson method [25]. The iterations to solve the simultaneous four equations are ($\hat{b} = b_r - ib_i, \hat{s} = s_r + is_i$)

$$\begin{bmatrix} b_r \\ b_i \\ s_r \\ s_i \end{bmatrix}_{j+1} = \begin{bmatrix} b_r \\ b_i \\ s_r \\ s_i \end{bmatrix}_{j} - \begin{bmatrix} \mathrm{Re}\left\{\frac{\partial \hat{w}(x_1)}{\partial b_r}, \frac{\partial \hat{w}(x_1)}{\partial b_i}, \frac{\partial \hat{w}(x_1)}{\partial s_r}, \frac{\partial \hat{w}(x_1)}{\partial s_i}\right\} \\ \mathrm{Im}\left\{\frac{\partial \hat{w}(x_1)}{\partial b_r}, \frac{\partial \hat{w}(x_1)}{\partial b_i}, \frac{\partial \hat{w}(x_1)}{\partial s_r}, \frac{\partial \hat{w}(x_1)}{\partial s_i}\right\} \\ \mathrm{Re}\left\{\frac{\partial \hat{w}(x_2)}{\partial b_r}, \frac{\partial \hat{w}(x_2)}{\partial b_i}, \frac{\partial \hat{w}(x_2)}{\partial s_r}, \frac{\partial \hat{w}(x_2)}{\partial s_i}\right\} \\ \mathrm{Im}\left\{\frac{\partial \hat{w}(x_2)}{\partial b_r}, \frac{\partial \hat{w}(x_2)}{\partial b_i}, \frac{\partial \hat{w}(x_2)}{\partial s_r}, \frac{\partial \hat{w}(x_2)}{\partial s_i}\right\} \end{bmatrix}^{-1} \begin{bmatrix} \mathrm{Re}\{\hat{w}(x_1) - w_0\Lambda_1 e^{i\phi_1}\} \\ \mathrm{Im}\{\hat{w}(x_1) - w_0\Lambda_1 e^{i\phi_1}\} \\ \mathrm{Re}\{\hat{w}(x_2) - w_0\Lambda_2 e^{i\phi_2}\} \\ \mathrm{Im}\{\hat{w}(x_2) - w_0\Lambda_2 e^{i\phi_2}\} \end{bmatrix}, \tag{9}$$

where the subscripts j and $j+1$ denote the current and next iterations, respectively. Symbolic computations to solve Eq. (6) and to calculate the derivatives with respect to $\hat{b}$ and $\hat{s}$ in Eq. (9) were performed using commercially available software MATLAB®. The flexural wave speed is derived from the characteristic mechanical impedances by considering harmonic flexural waves propagating in the plate such that the displacement and rotation is given as $w(x,t) = \mathrm{Re}\{\hat{B}e^{i(\omega t + \hat{b}\hat{\beta}x)}\}$ and $\psi_x(x,t) = \mathrm{Re}\{i\hat{k}_1\hat{B}e^{i(\omega t+\hat{b}\hat{\beta}x)}\}$, respectively, and is obtained as [26]

$$\hat{c} = c(1 + i\eta_c) = \frac{\hat{D}\hat{b}}{M_b\hat{\beta}\omega} = \frac{\omega}{\hat{b}\hat{\beta}}. \tag{10}$$

Consequently, the wave speed is calculated using the converged values of $\hat{b}$ and $\hat{s}$. The flexural wave speed is complex when there is a damping in the structure. For the Timoshenko beam, the flexural deformation occurs as bending at low frequencies. At high frequencies, the shear modes of vibration dominate [26]. When the beam response is dominated only by the bending or shear modes of vibration, the application of the transfer function method of the Timoshenko beam requires impractically precise measurement of the transfer functions as shown in the sensitivity analysis presented in later sections. In such cases, the application of the classical beam or the shear beam theories is preferred.

2.3. The classical beam

For vibration of a beam of a small thickness, the effects from the shear deformation and the rotary inertia are negligibly small compared to those of the bending deformation. In such cases,

the equation of motion is simplified to that of the classical beam [27]

$$D\,\frac{\partial^4 w}{\partial x^4} + M_b\,\frac{\partial^2 w}{\partial t^2} = 0. \tag{11}$$

The satisfying beam function is

$$\hat{w}(x) = \hat{A}_1 \sin \hat{k}_b x + \hat{A}_2 \cos \hat{k}_b x + \hat{A}_3 \mathrm{e}^{\hat{k}_b(x-L)} + \hat{A}_4 \mathrm{e}^{-\hat{k}_b x}, \tag{12}$$

where $\hat{k}_b$ is the wavenumber related to the circular frequency through $\hat{k}_b = (\omega^2 M_b/\hat{D})^{1/4}$. Four boundary conditions of the clamped–free beam are

$$\hat{w}(0) = w_0, \quad \frac{\partial \hat{w}(0)}{\partial x} = 0, \quad \frac{\partial^2 \hat{w}(L)}{\partial^2 x} = 0, \quad \frac{\partial^3 \hat{w}(L)}{\partial^3 x} = 0. \tag{13a–d}$$

The following matrix system of equations is obtained from Eqs. (12) and (13) as

$$\begin{bmatrix} 0 & 1 & \mathrm{e}^{-\hat{k}_b L} & 1 \\ 1 & 0 & \mathrm{e}^{-\hat{k}_b L} & -1 \\ -\sin \hat{k}_b L & -\cos \hat{k}_b L & 1 & \mathrm{e}^{-\hat{k}_b L} \\ -\cos \hat{k}_b L & \sin \hat{k}_b L & 1 & -\mathrm{e}^{-\hat{k}_b L} \end{bmatrix} \begin{bmatrix} \hat{A}_1 \\ \hat{A}_2 \\ \hat{A}_3 \\ \hat{A}_4 \end{bmatrix} = \begin{bmatrix} w_0 \\ 0 \\ 0 \\ 0 \end{bmatrix}. \tag{14}$$

Similar to the procedures applied for the Timoshenko beam, the above matrix system of equations is solved using the symbolic calculations to obtain the transfer function between the displacements. The complex wavenumber is obtained through the Newton–Rapson method, and the bending stiffness is consequently calculated as

$$\hat{D} = \frac{\omega^2 M_b}{\hat{k}_b^4}. \tag{15}$$

Only one transfer function measurement is required

$$\Lambda_1 \mathrm{e}^{\mathrm{i}\phi_1} = \frac{\hat{w}(x_1)}{\hat{w}(0)} = \frac{\hat{A}_1 \sin \hat{k}_b x_1 + \hat{A}_2 \cos \hat{k}_b x_1 + \hat{A}_3 \mathrm{e}^{\hat{k}_b(x_1-L)} + \hat{A}_4 \mathrm{e}^{-\hat{k}_b x_1}}{w_0}. \tag{16}$$

Then, the Newton–Rapson method is applied to solve Eq. (16) with respect to the complex wavenumber, $\hat{k}_b = k_{br} - \mathrm{i}k_{bi}$, numerically. The iterations to solve the above equation are performed as

$$\begin{bmatrix} k_{br} \\ k_{bi} \end{bmatrix}_{j+1} = \begin{bmatrix} k_{br} \\ k_{bi} \end{bmatrix}_{j} - \begin{bmatrix} \mathrm{Re}\left\{ \dfrac{\partial \hat{w}(x_1)}{\partial k_{br}}, \dfrac{\partial \hat{w}(x_1)}{\partial k_{bi}} \right\} \\ \mathrm{Im}\left\{ \dfrac{\partial \hat{w}(x_1)}{\partial k_{br}}, \dfrac{\partial \hat{w}(x_1)}{\partial k_{bi}} \right\} \end{bmatrix}^{-1} \begin{bmatrix} \mathrm{Re}\{\hat{w}(x_1) - w_0 \Lambda_1 \mathrm{e}^{\mathrm{i}\phi_1}\} \\ \mathrm{Im}\{\hat{w}(x_1) - w_0 \Lambda_1 \mathrm{e}^{\mathrm{i}\phi_1}\} \end{bmatrix}. \tag{17}$$

2.4. The shear beam

When the bending deformation is negligibly small and the flexural displacement of the panel occurs through the shear modes (the shear beam, Fig. 1(c)), the equation of

motion is

$$S\,\frac{\partial^2 w}{\partial x^2} = M_b\,\frac{\partial^2 w}{\partial t^2}. \tag{18}$$

The satisfying beam functions are

$$\hat{w}(x) = \hat{A}_1 \sin \hat{k}_b x + \hat{A}_2 \cos \hat{k}_b x, \tag{19}$$

where the wavenumber $\hat{k}_b$ is related to the circular frequency through $\hat{k}_b = \omega\sqrt{M_b/\hat{S}}$. Note that there are no exponentially decaying (evanescent) waves for the shear beam. After applying the fixed–free boundary conditions, the transfer function is obtained as

$$A_1 e^{i\phi_1} = \frac{\hat{w}(x_1)}{\hat{w}(0)} = \cos \hat{k}_b(L - x)/\cos \hat{k}_b L. \tag{20}$$

For the shear beam, the unknown complex wavenumber is calculated through the transfer function method, and the complex shear stiffness is obtained consequently. The Newton–Rapson method is applied to solve Eq. (20) after separating the real and imaginary parts.

2.5. Different boundary conditions

In the transfer function methods, the geometric boundary conditions are preferred rather than the natural boundary conditions to minimize computational costs. If the beam is supported by springs of unknown stiffness, the complexity of the problem increases significantly. Consequently, the geometric boundary conditions such as the free or clamped boundary conditions are preferred. The geometric boundary conditions are relatively simple to implement in laboratory setups. The same numerical procedures apply to beams with different boundary conditions than those considered in previous sections. For example, the boundary conditions of the impact hammer tests, Fig. 2(c), for the Timoshenko beam, are

$$\frac{\partial \hat{w}(0)}{\partial x} - \hat{\psi}_x(0) = -\frac{F_0}{\hat{S}}, \quad \frac{\partial \hat{\psi}_x(0)}{\partial x} = 0, \quad \frac{\partial \hat{w}(L)}{\partial x} - \hat{\psi}_x(L) = 0, \quad \frac{\partial \hat{\psi}_x(L)}{\partial x} = 0, \tag{21a–d}$$

where F_0 is the impact force applied at $x = 0$.

Large variations of the boundary conditions other than the clamped–free beam are possible [24]. The transfer function depends also on the kinds of the excitation method. Thereby a lot of variations on the boundary conditions in deriving the transfer functions are possible. After obtaining the beam functions for each boundary condition, the transfer function methods are applied in the exactly same procedures as presented in this section.

3. Sensitivity analysis

Measurement inaccuracies of the experimental variables, for example—calibration error in vibration measurements, misaligned sensor locations, length-wise variation of the beam geometry, non-identical frequency-dependent characteristics of the sensors, electrical noise, and incoherent measurements, etc., are inevitable. Structural vibrations which do not conform to those assumed

in deriving the linear equation of motion also contribute to the inaccuracy. The sensitivity of the proposed transfer function to these errors depends on several factors including dynamic mechanical properties and vibrational characteristics of the beam. For example, when the beam vibration is primarily influenced by the shear modes, Fig. 1(b), measuring the bending stiffness using the transfer function method of the Timoshenko beam is very sensitive to the inaccurate measurements. The solution of the Newton–Rapson methods may not converge or may result in physically unacceptable values (for example, negative stiffness) when the sensitivities are too large.

The sensitivity of the measured dynamic mechanical properties to the experimental variables, are derived following the procedures similar to those used for the transfer function method for the longitudinal vibration of the rods presented in Ref. [11]. For the Timoshenko beam, the sensitivities are derived from Eq. (7) as

$$\begin{bmatrix} \mathrm{d}D_r \\ \mathrm{d}D_i \\ \mathrm{d}S_r \\ \mathrm{d}S_i \end{bmatrix} = -2\omega^2 M_b \begin{bmatrix} \mathrm{Re}\{\hat{b}^{-3}(1,-\mathrm{i}),0,0\} \\ \mathrm{Im}\{\hat{b}^{-3}(1,-\mathrm{i}),0,0\} \\ \mathrm{Re}\{\hat{s}^{-2}\hat{b}^{-3}(1,-\mathrm{i}),\hat{s}^{-3}\hat{b}^{-2}(1,-\mathrm{i})\} \\ \mathrm{Im}\{\hat{s}^{-2}\hat{b}^{-3}(1,-\mathrm{i}),\hat{s}^{-3}\hat{b}^{-2}(1,-\mathrm{i})\} \end{bmatrix} \begin{bmatrix} \mathrm{d}b_r \\ \mathrm{d}b_i \\ \mathrm{d}s_r \\ \mathrm{d}s_i \end{bmatrix}. \tag{22}$$

Consequently, the sensitivity of the dynamic mechanical properties are calculated from the sensitivity of $\hat{b}$ and $\hat{s}$ to the measured transfer function which are obtained from Eq. (8) as

$$\begin{bmatrix} \mathrm{d}b_r \\ \mathrm{d}b_i \\ \mathrm{d}s_r \\ \mathrm{d}s_i \end{bmatrix} = w_0 \begin{bmatrix} \mathrm{Re}\left\{\dfrac{\partial\hat{w}(x_1)}{\partial b_r}\ \dfrac{\partial\hat{w}(x_1)}{\partial b_i}\ \dfrac{\partial\hat{w}(x_1)}{\partial s_r}\ \dfrac{\partial\hat{w}(x_1)}{\partial s_i}\right\} \\ \mathrm{Im}\left\{\dfrac{\partial\hat{w}(x_1)}{\partial b_r}\ \dfrac{\partial\hat{w}(x_1)}{\partial b_i}\ \dfrac{\partial\hat{w}(x_1)}{\partial s_r}\ \dfrac{\partial\hat{w}(x_1)}{\partial s_i}\right\} \\ \mathrm{Re}\left\{\dfrac{\partial\hat{w}(x_2)}{\partial b_r}\ \dfrac{\partial\hat{w}(x_2)}{\partial b_i}\ \dfrac{\partial\hat{w}(x_2)}{\partial s_r}\ \dfrac{\partial\hat{w}(x_2)}{\partial s_i}\right\} \\ \mathrm{Im}\left\{\dfrac{\partial\hat{w}(x_2)}{\partial b_r}\ \dfrac{\partial\hat{w}(x_2)}{\partial b_i}\ \dfrac{\partial\hat{w}(x_2)}{\partial s_r}\ \dfrac{\partial\hat{w}(x_2)}{\partial s_i}\right\} \end{bmatrix}^{-1} \begin{bmatrix} \mathrm{Re}\{\mathrm{e}^{\mathrm{i}\phi_1},\mathrm{i}\Lambda_1\mathrm{e}^{\mathrm{i}\phi_1},0,0\} \\ \mathrm{Im}\{\mathrm{e}^{\mathrm{i}\phi_2},\mathrm{i}\Lambda_1\mathrm{e}^{\mathrm{i}\phi_1},0,0\} \\ \mathrm{Re}\{0,0,\mathrm{e}^{\mathrm{i}\phi_2},\mathrm{i}\Lambda_2\mathrm{e}^{\mathrm{i}\phi_2}\} \\ \mathrm{Im}\{0,0,\mathrm{e}^{\mathrm{i}\phi_2},\mathrm{i}\Lambda_2\mathrm{e}^{\mathrm{i}\phi_2}\} \end{bmatrix} \begin{bmatrix} \mathrm{d}\Lambda_1 \\ \mathrm{d}\phi_1 \\ \mathrm{d}\Lambda_2 \\ \mathrm{d}\phi_1 \end{bmatrix}. \tag{23}$$

Similar procedures are repeated for the classical and the shear beams, and the sensitivities are derived, respectively as

$$\begin{bmatrix} \mathrm{d}D_r \\ \mathrm{d}D_i \end{bmatrix} = -4\omega^2 M_b w_0 \begin{bmatrix} \mathrm{Re}\{\hat{k}_b^{-5}(1,-\mathrm{i})\} \\ \mathrm{Im}\{\hat{k}_b^{-5}(1,-\mathrm{i})\} \end{bmatrix} \begin{bmatrix} \mathrm{Re}\left\{\dfrac{\partial\hat{w}(x_1)}{\partial k_{br}}\ \dfrac{\partial\hat{w}(x_1)}{\partial k_{bi}}\right\} \\ \mathrm{Im}\left\{\dfrac{\partial\hat{w}(x_1)}{\partial k_{br}}\ \dfrac{\partial\hat{w}(x_1)}{\partial k_{bi}}\right\} \end{bmatrix}^{-1} \begin{bmatrix} \mathrm{Re}\{\mathrm{e}^{\mathrm{i}\phi_1},\mathrm{i}\Lambda_1\mathrm{e}^{\mathrm{i}\phi_1}\} \\ \mathrm{Im}\{\mathrm{e}^{\mathrm{i}\phi_1},\mathrm{i}\Lambda_1\mathrm{e}^{\mathrm{i}\phi_1}\} \end{bmatrix} \begin{bmatrix} \mathrm{d}\Lambda_1 \\ \mathrm{d}\phi_1 \end{bmatrix}, \tag{24a}$$

$$\begin{bmatrix} \mathrm{d}S_r \\ \mathrm{d}S_i \end{bmatrix} = -2\omega^2 M_b w_0 \begin{bmatrix} \mathrm{Re}\{\hat{k}_b^{-3}(1,-\mathrm{i})\} \\ \mathrm{Im}\{\hat{k}_b^{-3}(1,-\mathrm{i})\} \end{bmatrix} \begin{bmatrix} \mathrm{Re}\left\{\dfrac{\partial \hat{w}(x_1)}{\partial k_{br}} \dfrac{\partial \hat{w}(x_1)}{\partial k_{bi}}\right\} \\ \mathrm{Im}\left\{\dfrac{\partial \hat{w}(x_1)}{\partial k_{br}} \dfrac{\partial \hat{w}(x_1)}{\partial k_{br}}\right\} \end{bmatrix}^{-1} \begin{bmatrix} \mathrm{Re}\{\mathrm{e}^{\mathrm{i}\phi_1}, \mathrm{i}\Lambda_1 \mathrm{e}^{\mathrm{i}\phi_1}\} \\ \mathrm{Im}\{\mathrm{e}^{\mathrm{i}\phi_1}, \mathrm{i}\Lambda_1 \mathrm{e}^{\mathrm{i}\phi_1}\} \end{bmatrix} \begin{bmatrix} \mathrm{d}\Lambda_1 \\ \mathrm{d}\phi_1 \end{bmatrix}. \tag{24b}$$

Other noise sources are discontinuities in beam construction and 2D vibration of the beam. To analyze the 2D effects, numerical methods such as the finite element or the Rayleigh–Ritz methods are required in most cases. These numerical methods are not appropriate in the transfer function method since the method requires closed-form solutions. Consequently, the width of the beam should be small compared to the wavelength. Also, experimental error from the location and finite size of the sensors should be minimized. In actual measurements, there are several more complicating factors such as the limited dynamic range of the sensors that induce measurement problems at anti-resonances especially when the damping in the system is small.

4. Results and discussions

4.1. Sensitivity analysis

The sensitivity analysis of the proposed methods was simulated for the beams considered in this study. The dynamic and geometric properties are shown in Table 1. Three sandwich beams with different core materials were custom-built. The first and second sandwich beams consisting of two identical thin face aluminum sheets of 0.4 mm thickness, and Nomex® honeycomb cores of 25.4 and 19 mm thickness, respectively. The widths of the sandwich honeycomb beams were 76.2 mm. The third sandwich beam consisted of two identical thin face aluminum sheets of 0.51 mm thickness, and a 25.4 mm thick foam core. The width of this sandwich beam was 74.2 mm. A polymeric beam, 51 mm diameter cylindrical bar made of Plexiglas® (beam 4), was also tested. Table 1 shows the length and measurement locations (x_1 and x_2) and the dynamic mechanical properties that were rough estimates from comparison of the measured transfer function and resonant frequencies with the predictions.

Table 1
Mechanical properties of beams and coordinates of vibration measurement

Beam No	M_b (kg/m)	I_b (10^{-6} kg m)	L (m)	x_1 (m)	x_2 (m)	D (Nm^2)	η_D (%)	S (kN)	η_S (%)
1 (sandwich-honeycomb)	0.33	38	0.84	0.33	0.58	750	0.1	105	2.0
2 (sandwich-honeycomb)	0.27	19	0.81	0.30	0.56	422	0.2	39	2.5
3 (sandwich-foam core)	0.37	45	0.77	0.26	0.52	946	0.18	10.2	2.6
4 (polymer)	2.41	390	0.70	0.23	0.47	1550	6.0	3200	6.0
5 (hollow cylinders)	0.30	215	0.89	0.25	0.50	540	0.1	1708	0.1

In deriving the solution of the Timoshenko beam, the beam functions in Eq. (4) are valid until

$$\left[(r^2-\hat{s}^2)^2+\frac{4}{\hat{b}^2}\right]^{1/2}>(r^2+\hat{s}^2). \tag{25}$$

The beams 1–4 in Table 1 satisfy the condition of Eq. (25) up to the frequencies, 8400, 7200, 2400, and 14,400 Hz, respectively. The analysis using Timoshenko beam theory was performed below these frequencies.

The calculated transfer functions for the second sandwich honeycomb beam (beam 2) from Eq. (6) are plotted in Fig. 3 using the parameters in Table 1. Fig. 4 shows the predicted flexural wave speeds of this beam obtained using Eq. (10). The bending and shear wave speeds assuming the bending and shear beams, respectively, are plotted also. The comparison suggested that the beam vibration was affected mostly by the bending modes at low frequencies. The shear modes of vibration dominated at high frequencies. In between these two extreme cases, both of the bending and shear modes of vibration influenced the beam response.

The sensitivity analysis was performed using the parameters in Table 1. The results for the honeycomb beam (beam 2) and the polymer beam (beam 4) are presented in Fig. 5. In most cases, the maximum peaks in the calculated sensitivities occurred at frequency ranges in which the differences of magnitudes and phases of the acceleration measurements are small. The sensitivities for the Timoshenko beam was low in the limited frequency ranges where bending and shear deformation occurs simultaneously, Fig. 5(a). When the shear deformation is small, for example the polymer beam (beam 4), the sensitivity of the obtained shear stiffness using the Timoshenko

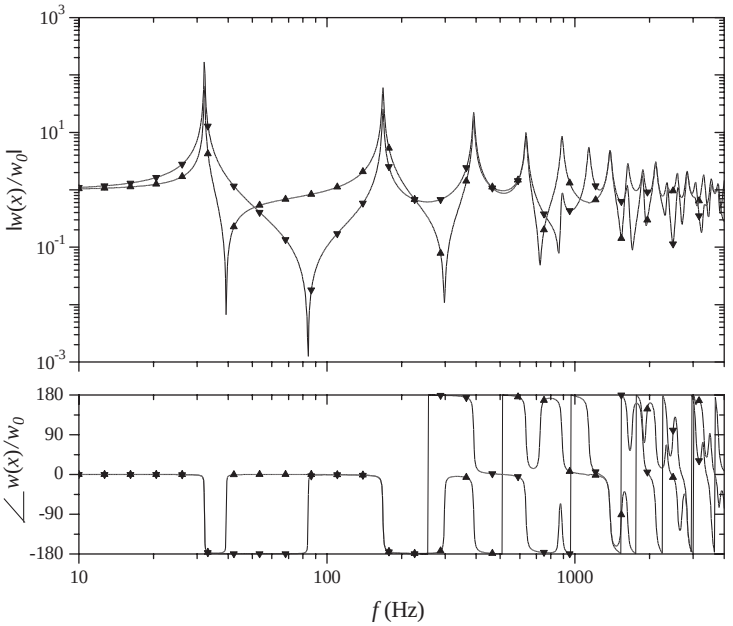

Fig. 3. Calculated transfer functions between transverse displacements at $x = x_0$ and $x =$:—▲—, x_1; —▼—, x_2.

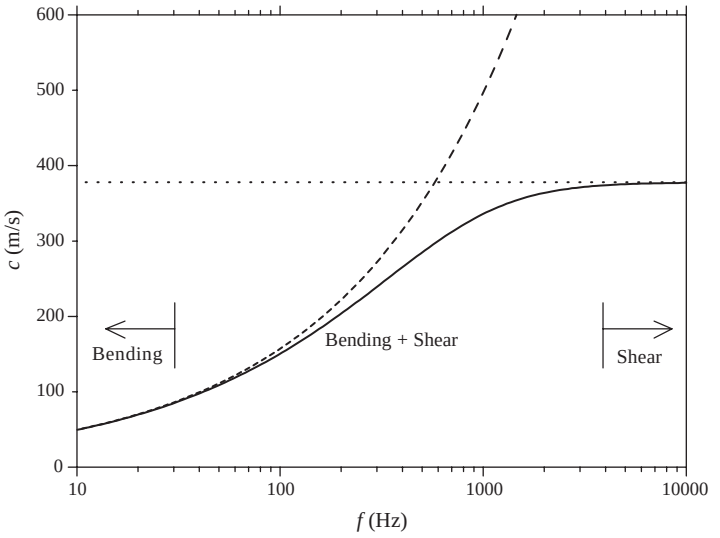

Fig. 4. Predicted flexural wave speeds of the honeycomb beam (beam 2):, ———, flexural wave speed; – – – – –, $c_b = (\omega^2 D/M_b)^{0.25}$; · · · · · ·, $c_s = \sqrt{S/M_b}$.

beam was larger than those of the bending stiffness. The calculated dynamic stiffnesses may not be physically acceptable in case the sensitivities are too large. In such cases, the solution from the Newton–Rapson method may diverge when small errors are included in the measured transfer function. In Figs. 5(b) and (c) which show simulation results for the same beam but for different beam equation of motion, the sensitivity for the classical beam was smaller in general compared to those obtained for the Timoshenko beam over the entire frequency ranges. The sensitivity analysis presented in this section is useful in analyzing the measured dynamic stiffness from the developed transfer function methods especially when physically unacceptable frequency-dependent behavior is observed as discussed later in this section.

Fig. 6 shows the sensitivity calculated assuming the classical beam and its variation with the location of the vibration measurements, x_1. The parameters of the honeycomb beam (beam 2) in Table 1 were applied. At locations and frequencies of the sensitivity maximum peaks, the results from the transfer function methods were excessively sensitive to the experimental errors. Consequently, the results were not reliable when obtained at frequencies of these peaks. The maximum peaks were more distinctive for test materials of small loss factor. For materials with large loss factor, the maximum peaks were broad, and consequently the results were less sensitive to the experimental variables at frequencies of these maximum peaks. When the location of the vibration measurement of the beam was too close to the fixed end of the beam, i.e., $x_1 \approx 0$, the sensitivity was large since the phase and magnitude difference between the two vibration measurements at $x = 0$ and x_1 was small. To avoid this large sensitivity to experimental variables, it would be advantageous to locate the sensors as far as possible, for example, the vibration measurements of the beam at the opposite ends ($x_1 = L$). However, this resulted in larger number of maximum peaks as shown in Fig. 6. A smaller number of peaks resulted as the location of the vibration measurements of the beam (x_1) approaches the one at the source. For example, first

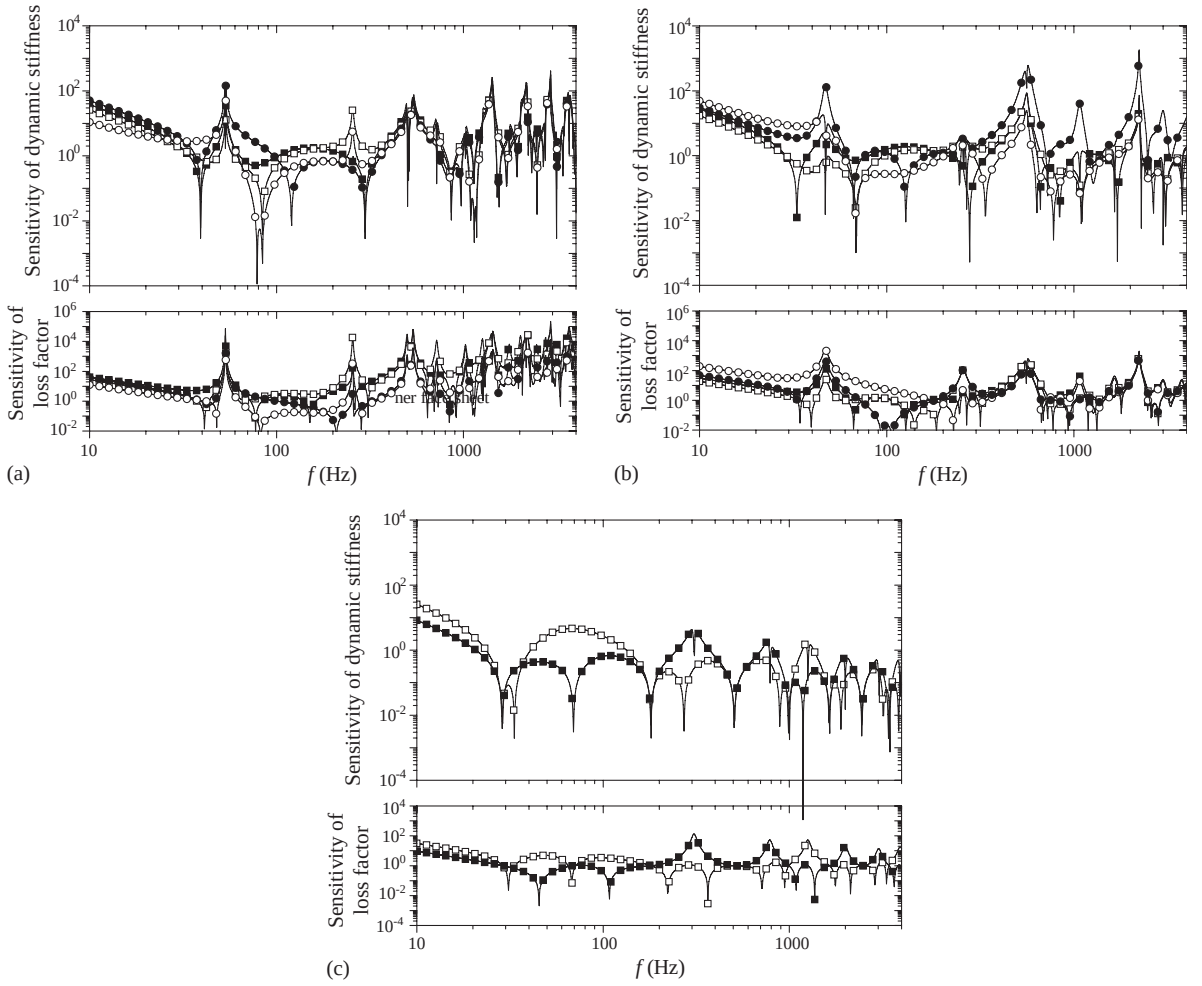

Fig. 5. Sensitivity on the amplitudes of the measured transfer function for the transfer function method of different equation of motion—Timoshenko beam theory applied (a) for sandwich beam (beam 2) and (b) for Plexiglas (beam 4), and (c) classical beam theory applied for Plexiglas (beam 4). Sensitivity of the dynamic stiffness: —■—, $(\partial D/\partial \Lambda_1)/(D/\Lambda_1)$; —□—, $(\partial D/\partial \Lambda_2)/(D/\Lambda_2)$; —●—, $(\partial S/\partial \Lambda_1)/(S/\Lambda_1)$; —○—, $(\partial S/\partial \Lambda_2)/(S/\Lambda_2)$, and same line parameters for the sensitivity of the loss factor, i.e., —■—, $(\partial \eta_D/\partial \Lambda_1)/(\eta_D/\Lambda_1)$.

sensitivity maximum peak occurred at $f = 1400$ Hz when $x_1 = L/3$, however four maximum peaks occurred at $f = 93$, 370, 830, 1490 Hz when $x_1 = L$. Consequently, it is recommended to avoid locating the sensor too close to the boundaries when excited under the fixed–free boundary condition.

4.2. Measurements of dynamic properties of complex structures

The experiments were performed to measure the dynamic mechanical properties of the beams in Table 1. A slip table (Unholtz-Dickie T-1000 Shaker) was used to induce controlled vibration of

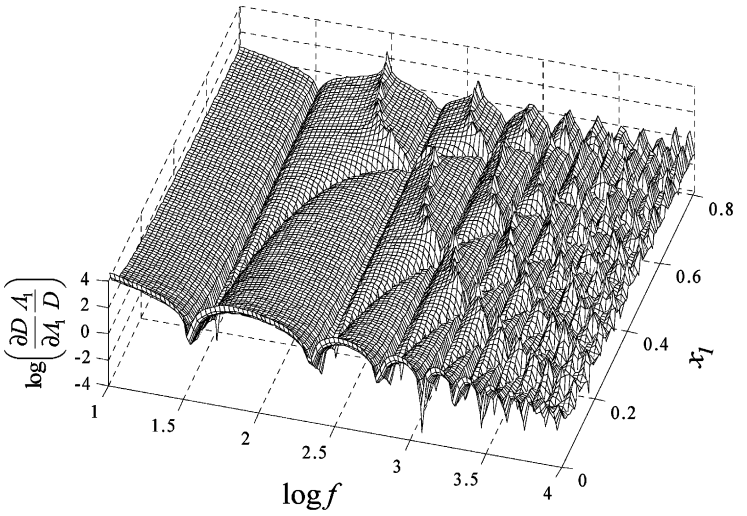

Fig. 6. Sensitivity of the bending stiffness for the transfer function method of the classical beam, and its variation with the location of the vibration measurements.

the beams under fixed–free boundary conditions (the slip table test). For the sandwich beams, an aluminum block of same thickness as the core replaced the core material at one end of the beam. The portion of the beam with the aluminum block was fixed to the slip table floor using a clamp made of steel. For the polymer beam (beam 4), one end of the beam was fixed to the slip table floor using an epoxy from which the same boundary conditions were imposed. Fig. 7 shows the experimental setup for the slip table tests. From the vibration of the slip table, the displacement boundary conditions of the beam were imposed as shown in Fig. 2(b).

Fig. 8 shows the measured transfer functions between the displacements for the sandwich honeycomb beam (beam 2). Miniature piezoelectric accelerometers (Endevco model 2250-A) were used to measure the acceleration. The frequency range of the random excitation was limited from 10 to 1400 Hz for the sandwich beams and from 10 to 2000 Hz for the polymer beam. The dynamic range of the slip table limited the frequency ranges to 2 kHz. The acceleration levels along the width of the sandwich beam near the fixture were not constant but became greater with increasing distance from the slip table floor at high frequencies due to non-rigid responses of the test fixture. To minimize the effects of this variation, the accelerometers were attached as close to the center of the beam width as possible.

Fig. 9 shows the measured complex stiffnesses of the beams (bending and shear stiffnesses and their loss factors) from the transfer function method of the Timoshenko beam and the slip table tests. The dashed lines are the rough estimates shown in Table 1 that were used as initial values for the Newton–Rapson method. The bending stiffness of the sandwich beams was almost constant and its loss factor was small since the aluminum face panel whose material damping is small had most significant impact on the bending stiffness. The obtained bending stiffness was very close to the value predicted from the properties of the face panel and the core thickness, d, as $D = E_f h d^2/2$

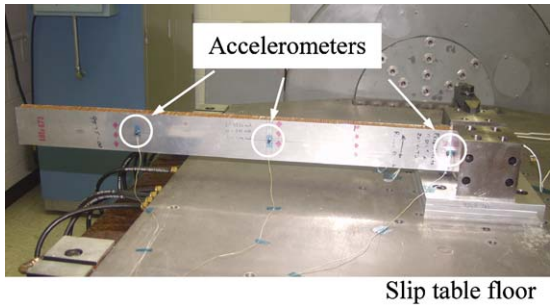

Fig. 7. Experimental setup of the slip table tests.

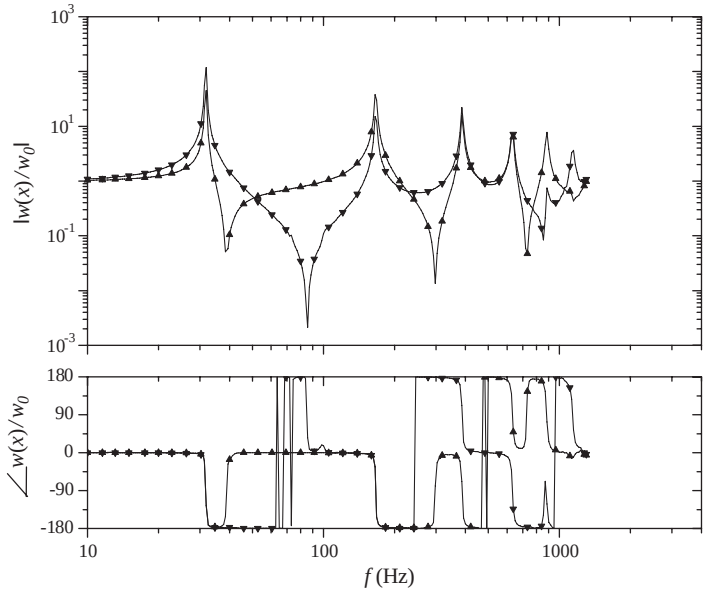

Fig. 8. Measured transfer functions for the honeycomb beam (beam 2). Same line parameters as in Fig. 3.

[1] where E_f is the Young's modulus and h is the thickness of the face panel. The shear loss factors of the sandwich beams were higher than those of the bending stiffnesses. A large variation of the measured shear loss factor was resulted for the sandwich beams of honeycomb core (beams 1 and 2) except the frequency ranges that the bending and shear deformation occurred simultaneously and consequently the sensitivities were low (100–300 Hz). There were several reasons for this large variation. The shear deformation occurred at high frequencies in which the sensitivity was large. Non-uniform lengthwise variations of the width of the core that were present in the custom-built honeycomb beams also contributed to the large variation.

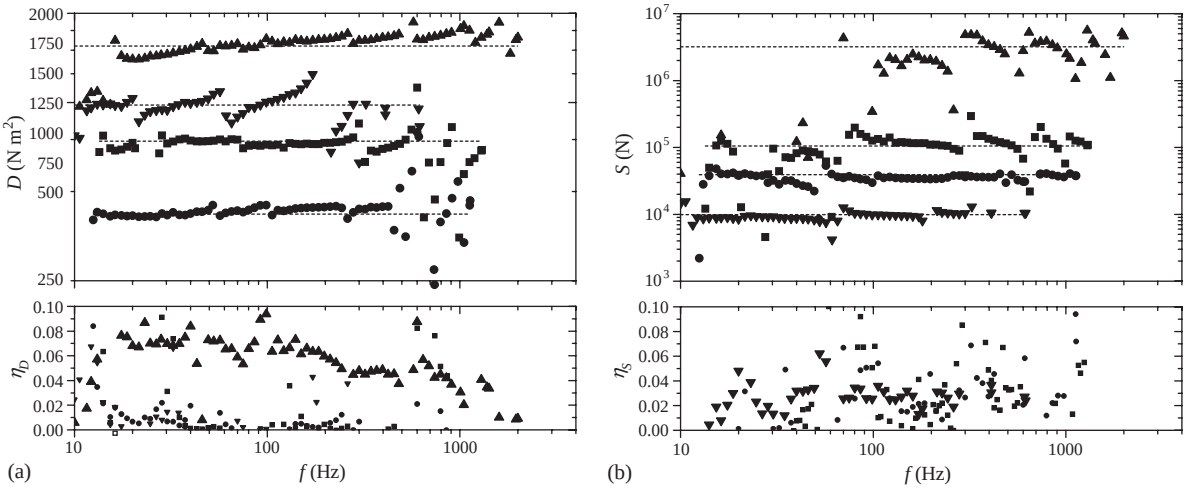

Fig. 9. (a) Bending and (b) shear stiffnesses measured from the transfer function method of the Timoshenko beam for different beams: ■, beam 1; ●, beam 2; ▲, beam 3; ▼, beam 4. The dashed lines represents values in Table 1.

In Fig. 9, there are discontinuities in the measured frequency-dependent variation of the measured dynamic stiffness and loss factors, for example, at 50 and 250 Hz for the sandwich beam (beam 2) and 50, 250, 600, and 1050 Hz for the polymer beam (beam 4). These frequencies correspond to the maximum peaks of the sensitivities in Fig. 5. Consequently, this discontinuous behavior in the measured dynamic characteristics is not avoidable especially when the material damping is small as discussed in the previous section.

Since the frequency range of the slip table tests was limited to 2 kHz, impact hammer tests were performed for the clamped–free beam to investigate the response of the sandwich beams. The impact hammer model PCB 086C80 was used to excite the clamped–free beam at the free end, $x = L$. The transfer functions between the beam responses $x = L$ and $x = x_1$ and x_2 were measured, and the transfer function methods were applied following the same procedures. For the impact hammer test the non-ideal and non-consistent impact forces and smaller number of averages compared to the slip table test were inevitable. The measured shear stiffnesses from the transfer function method of the shear beam and the impact hammer tests are shown in Fig. 10. The application of the shear beam was valid only at high frequencies in which the measured shear stiffness was almost constant and agreed well to those calculated assuming the Timoshenko beam. This suggested that the application of the shear beam is an appropriate alternative to the Timoshenko beam at these high frequencies.

Fig. 11 shows the flexural wave speeds calculated from Eq. (10) and the values measured from the slip table tests assuming the Timoshenko beam. The dashed lines are the calculated values using the values in Table 1. The wave speeds measured from the impact hammer tests assuming the shear beam are plotted also (the unfilled keys). For all the beams tested in this study, the wave speeds smoothly increased with frequency. At high frequencies, the wave speeds were almost constant for the sandwich beams due to the shear deformation. The measured wave speeds were

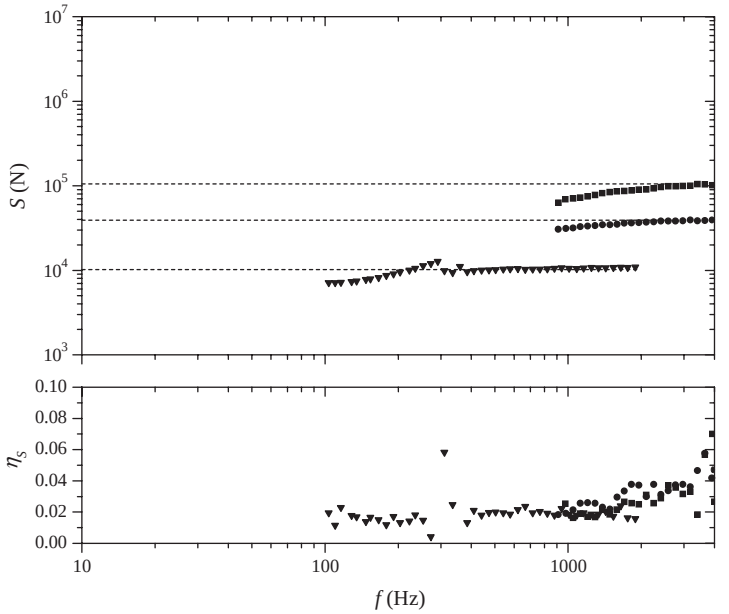

Fig. 10. The shear stiffness of the beams measured from the impact hammer tests. Same keys as in Fig. 9.

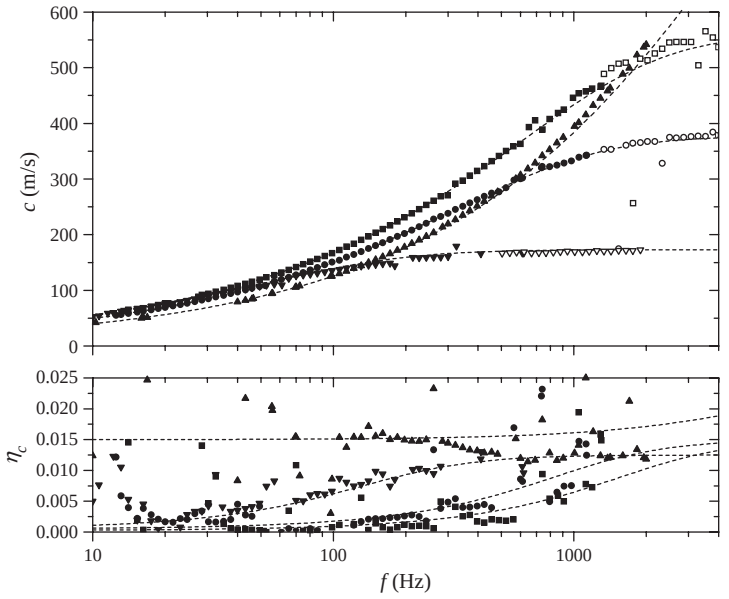

Fig. 11. Flexural wave speeds of the beams and their loss factors: the dashed lines are calculated values using properties in Table 1. Same keys as in Fig. 9. Filled keys—the slip table tests and the Timoshenko beam, and unfilled keys—the impact hammer tests and the shear beam.

not affected by independent face bending of the inner and outer laminates which Kurtze and Watters considered in analyzing the wave propagation through honeycomb panels [26,28]. At low frequencies, the wave speeds were close to those calculated through the classical beam. In between these two extreme cases, the beam vibrations were influenced both by the bending and shear modes. The loss factors of the wave speeds, η_c, are also shown. With increasing frequency, gradual changes of the measured loss factor from those affected by the bending stiffness of small loss factor to those affected by the shear stiffness of large loss factor were observed. For the polymer beam, the wave speeds increased constantly with frequency more rapidly than the values calculated using the properties in Table 1 due to the increasing bending stiffness in Fig. 9.

Fig. 12 shows the bending stiffness of the polymer beam (beam 4) obtained by the transfer function method of the classical beam and the slip table test. Since the sensitivity analysis presented in Fig. 5(c) suggests that there is no significant sensitivity maximum below 1 kHz, the measured transfer function at $x = x_1$ was used to obtain the dynamic characteristics. When the measured transfer function at $x = x_2$ was used, there was discontinuous variation at $f = 300$ Hz as predicted in the sensitivity analysis. The bending stiffness became larger with increasing frequency at frequencies lower than 300 Hz, and agreed well to the values calculated assuming the Timoshenko beam, Fig. 9(a). At higher frequencies, the stiffness measured assuming the classical beam started to decrease, which suggested that the shear deformation and the rotary inertia were no longer negligible and should be taken into consideration, i.e., the Timoshenko beam theory should be used as the results shown in Fig. 9(a). The bending stiffness had a loss factor less than 0.1 and continued to decreases with increasing frequency. This loss factor variation and Young's moduli obtained from the measured bending stiffness were very similar to those measured using different methods for the Plexiglas® in Ref. [29].

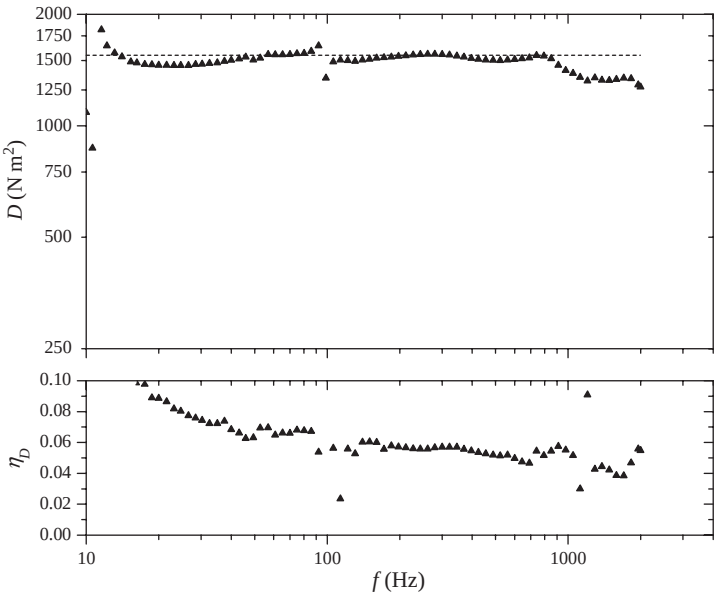

Fig. 12. The bending stiffness of the polymer beam measured from the transfer function methods and the classical beam.

4.3. Vibration damping using granular and porous materials

To investigate the damping of structures using porous and granular materials, the slip table tests were performed for hollow cylindrical beams (beam 5 in Table 1, o.d. and i.d. were 0.025 and 0.022 m, respectively), made of aluminum. One end of the beam was fixed to the slip table floor using an epoxy. The dynamic properties of beams with and without damping treatments in the beam cavity were measured. Polyurethane acoustic foam and three different lightweight microspheres were considered as damping materials. The particle radiuses of the three microsphere samples were 210, 300, 600 μm, and their densities were 44, 23, 23 kg/m^3, respectively. The particles were made of polyimide and had geometries close to a hollow sphere. The density of the polyurethane acoustic foam was 37 kg/m^3. The foam was cut to the shape of spherical cylinder whose diameter was slightly larger than the i.d. of the beam and was tightly fitted to the beam cavity without epoxy.

Fig. 13 shows the measured transfer functions between the displacement imposed by the vibration of the slip table floor (w_0) and the displacement at $x = x_1(w(x_1))$ when the beam cavity was empty, and was filled by the microspheres ($R = 210\,\mu m$). The mass ratio of the microspheres to the beam was 5%. This ratio decreased when the other lightweight microspheres of smaller density was tested. The lightweight microspheres significantly reduced the vibration response of the beam at resonances. Using the transfer function method of the classical beam, the dynamic stiffness was calculated from the measured transfer functions and is shown in Fig. 14. The conduction of the vibration energy into the granular material and subsequent dissipation increased the bending loss factor significantly. The maximum of the loss factor occurred when there was a resonance for the acoustic response along the cross-section. For the damping material

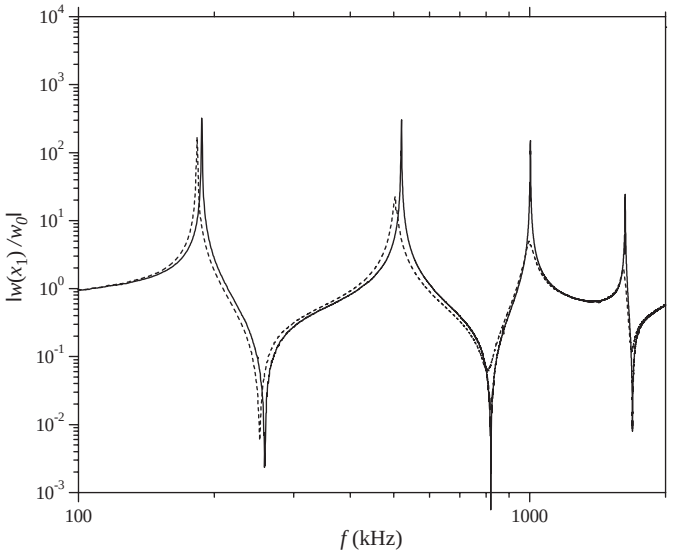

Fig. 13. Transfer function for the vibration of the beam: ———, without (un-damped) and - - - - - -, with (damped) microspheres ($R = 210\,\mu m$) inside the beam cavity.

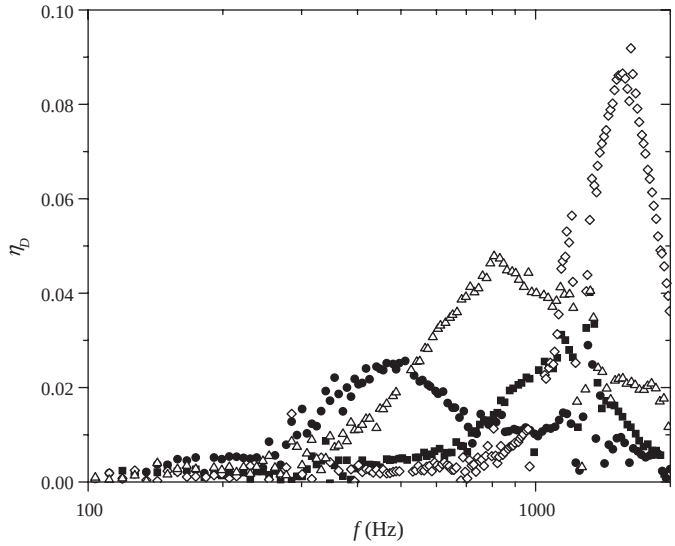

Fig. 14. Measured loss factors of the bending stiffness of the beam treated by different damping materials—lightweight microspheres, R: ● 600 μm; ■, 300 μm; ◇, 210 μm; and △, polyurethane acoustic foam.

with higher wave speed, for example the granular material with smaller density and particle size, the maximum loss factor occurred at higher frequencies. The analysis of this vibration control using granular materials together with the measurements of vibration characteristics of granular and porous materials is the continuing research subject of the author.

5. Conclusions

Transfer function methods to measure dynamic mechanical properties of beams were developed. Frequency-dependent wave speeds, bending and shear stiffness and their loss factors were measured. Different beam equations of motion, the Timoshenko beam, the classical beam, and the shear beam, were applied in the transfer function methods to predict and analyze the wave propagations. Sensitivity analysis of the developed transfer function method was performed to investigate the effects of experimental variables. The application of the Timoshenko beam to the transfer function method was required when the beam vibration was influenced by both the bending and shear modes. In case the beam vibration is affected by the bending or shear modes only, the application of the classical beam or the shear beam was advantageous from smaller sensitivity. Experiments were performed to measure dynamic mechanical properties of beams. For the transfer function method of the Timoshenko beam, the results were reliable when both the bending and shear modes of vibration occurred as was predicted from the sensitivity analysis. The wave speeds of the sandwich beam became larger with increasing frequency. At high frequencies, the measured wave speeds of the sandwich beams were almost constant as predicted from the

Timoshenko beam theory. The dynamic stiffness of structures damped by porous and granular materials was also investigated to study its large variation with frequency.

Only when the transfer function methods with adequate equation of motion were used, non-resonant frequency dependence of the wave speeds and dynamic mechanical properties were resulted. Although the number of vibration measurements was kept as small as possible in this study, increasing the number of vibration measurements and selecting the results of small sensitivity can improve the quality of the results. The measured dynamic properties can be used in the theoretical models of complex structures to predict their vibro-acoustic performance, and be compared to each other for various constructions.

Acknowledgements

The financial support from the NASA Langley Research Center while in residence under a NRC Post-doctoral Research Associateship Award is gratefully acknowledged. The author sincerely appreciates Dr. Richard J. Silcox for supervising this work and Daniel L. Palumbo, Dr. Ralph D. Buehrle, and Jacob Klos for many discussions and suggestions.

References

[1] D. Zenkert, *An Introduction to Sandwich Construction*, Chameleon Press, London, 1997.
[2] D.I.G. Jones, Temperature–frequency dependence of dynamic properties of damping materials, *Journal of Sound and Vibration* 33 (1974) 451–470.
[3] L.E. Kinsler, A.R. Frey, A.B. Coppens, J.V. Sanders, *Fundamentals of Acoustics*, Wiley, New York, 1982.
[4] J.D. Ferry, *Viscoelastic Properties of Polymers*, Wiley, New York, 1980.
[5] W.M. Madigosky, G.F. Lee, Automated dynamic Young's modulus and loss factor measurements, *Journal of the Acoustical Society of America* 66 (1979) 345–349.
[6] T. Pritz, Transfer function method for investigating the complex modulus of acoustic materials: rod-like specimen, *Journal of Sound and Vibration* 81 (1982) 359–376.
[7] W.M. Madigosky, G.F. Lee, Improved resonance technique for materials characterization, *Journal of the Acoustical Society of America* 73 (1983) 1374–1377.
[8] N. Lagakos, J. Jarzynski, J.H. Cole, J.A. Bucaro, Frequency and temperature dependence of elastic moduli of polymers, *Journal of Applied Physics* 59 (1986) 4017–4031.
[9] J.L. Buchanan, Numerical solution for the dynamic moduli of a viscoelastic bar, *Journal of the Acoustical Society of America* 81 (1986) 1775–1786.
[10] S. Sim, K.-J. Kim, A method to determine the complex modulus and Poisson's ratio of viscoelastic materials for FEM applications, *Journal of Sound and Vibration* 141 (1990) 71–82.
[11] T.-K. Ahn, K.-J. Kim, Sensitivity analysis for estimation of complex modulus of viscoelastic materials by non-resonance method, *Journal of Sound and Vibration* 176 (1994) 543–561.
[12] J. Park, T. Siegmund, L. Mongeau, Viscoelastic properties of foamed thermoplastic vulcanizates and their dependence on void fraction, *Cellular Polymers* 22 (2003) 137–156.
[13] ANSI S2.22-1998, *Resonance Method for Measuring the Dynamic Mechanical Properties of Viscoelastic Materials*, American National Standards Institute, Acoustical Society of America, New York, 1998.
[14] D.R. Bland, E.H. Lee, Calculation of the complex modulus of linear viscoelastic materials from vibrating reed measurements, *Journal of Applied Physics* 26 (1955) 1497–1503.
[15] S.A. Rizzi, J.F. Doyle, Determination of dynamic bending stiffness of an orthotropic cross-ply composite, *Mechanical Systems and Signal Processing* 1 (1987) 285–291.

[16] K. Grosh, E.G. Williams, Complex wave-number decomposition of structural vibrations, *Journal of the Acoustical Society of America* 93 (1993) 836–848.
[17] A.J. Hull, D.A. Hurdis, A parameter estimation method for the flexural wave properties of a beam, *Journal of Sound and Vibration* 262 (2003) 187–197.
[18] J.G. McDaniel, W.S. Shepard Jr., Estimation of structural wave numbers from spatially sparse response measurements, *Journal of the Acoustical Society of America* 108 (2000) 1674–1682.
[19] P.J. Halliday, K. Grosh, Maximum likelihood estimation of structural wave components from noisy data, *Journal of the Acoustical Society of America* 111 (2002) 1709–1717.
[20] W. Lins, G. Kaindl, H. Peterlik, K. Kromp, A novel resonant beam technique to determine the elastic moduli in dependence on orientation and temperature up to 2000 °C, *Review of Scientific Instruments* 70 (1999) 3052–3058.
[21] R.B. Thompson, G.A. Alers, D.O. Thompson, M.A. Tennison, Dispersion of flexural waves in honeycomb sandwich, *Journal of the Acoustical Society of America* 57 (1975) 1119–1127.
[22] T. Saito, R.D. Parbery, S. Okuno, S. Kawano, Parameter identification for aluminum honeycomb sandwich panels based on orthotropic Timoshenko beam theory, *Journal of Sound and Vibration* 208 (1997) 271–287.
[23] T. Pritz, Frequency dependences of complex moduli and complex Poisson's ratio of read solid materials, *Journal of Sound and Vibration* 214 (1998) 83–104.
[24] T.C. Huang, The effect of rotatory inertia and of shear deformation on the frequency and normal mode equations of uniform beams with simple end conditions, *Journal of Applied Mechanics* 28 (1961) 579–584.
[25] S.S. Rao, *Applied Numerical Methods for Engineers and Scientists*, Prentice-Hall, Upper Saddle River, NJ, 2002.
[26] J. Park, Wave propagation, vibration and sound radiation analysis of compliantly supported sandwich panels, *Journal of Sound and Vibration*, submitted.
[27] F. Fahy, *Sound and Structural Vibration: Radiation, Transmission and Response*, Academic Press, London, 1985.
[28] G. Kurtze, B.G. Watters, New wall design for high transmission loss or high damping, *Journal of the Acoustical Society of America* 31 (1959) 739–748.
[29] T. Lee, R.S. Lakes, A. Lal, Resonant ultrasound spectroscopy for measurement of mechanical damping: comparison with broadband viscoelastic spectroscopy, *Review of Scientific Instruments* 71 (2000) 2855–2861.